ELSEVIER

Colloids and Surfaces
A: Physicochemical and Engineering Aspects 167 (2000) 31–46

COLLOIDS AND SURFACES A

www.elsevier.nl/locate/colsurfa

Modeling self-assembly of surfactants at solid/liquid interfaces. I. Hydrophobic surfaces

Robert A. Johnson, R. Nagarajan *

161 Fenske Laboratory, Department of Chemical Engineering, The Pennsylvania State University, University Park, PA 16802-4400, USA

Abstract

A theory of surfactant self-assembly on isotropic hydrophobic surfaces is presented by extending the well established treatment of self-assembly in solution. The free-energy model for the formation of surface aggregates includes an additional term (beyond those used for bulk aggregates) to account for the replacement of the solid surface-water contact by the solid surface-aggregate core contact. This free-energy contribution is characterized by a single parameter, the displacement tension γ. Illustrative calculations of the critical aggregation concentration (CAC), aggregate shape and size are presented for anionic, zwitterionic, and nonionic surfactants. For all types of surfactants, the CAC is much lower than the bulk CMC. Regardless of the value of γ, surface aggregates of ionic surfactant are always smaller than the bulk-phase analogs. Conversely, surface aggregates of zwitterionic and nonionic surfactants can be either smaller or larger than those in solution, depending on the interplay between headgroup repulsion and aggregate core-solid surface attraction. A rich variety of aggregate morphologies including hemispheres, hemicylinders, finite disks, and continuous monolayers are predicted depending upon the surfactant and the solid surface. More interestingly, increasing the chemical potential of the surfactant (by increasing the total surfactant concentration) can induce the morphological transformation of surface aggregates to less energetically favorable structures. Thus the same surfactant on a given solid surface can self-assemble into various shapes depending upon the total surfactant concentration.

Keywords: Self assembly; Surfactants; Solid/liquid interfaces

1. Introduction

The adsorption of surfactants from solutions onto solid surfaces has been investigated over the years because of the numerous practical applications where solid-liquid contact occurs [1]. Both hydrophobic surfaces and hydrophilic surfaces carrying charges have been examined. It has been postulated that adsorbed surfactants will self-assemble at the solid/liquid interface in a manner analogous to bulk-phase micellization [2,3]. This is to be distinguished from the situation where micelles already formed in the bulk solution adsorb at the solid surface. The self-assembly at the solid/liquid interface is perturbed from the corresponding bulk-phase micellization due to compet-

* Corresponding author: Tel.: +1-814-863-1973; fax: +1-814-865-7846.

E-mail address: rxn@psu.edu (R. Nagarajan)

0927-7757/00/$ - see front matter
PII: S0927-7757(99)00481-1

ing surfactant-surface and solvent-surface interactions. This perturbation makes possible the formation of surface aggregates that can differ significantly in size and microstructure from those formed in the bulk.

Numerous studies, both theoretical and experimental, have been made concerning the adsorption behavior of surfactants. In general, the amount of surfactant adsorbed is measured or predicted as a function of the properties of the surfactant solution. On the theoretical side, the main approach has employed thermodynamic considerations to derive analytical representations of surfactant adsorption and two-dimensional condensation at solid surfaces [4–10]. In these studies, the microstructure of the adsorbed surfactant was taken to be lamellar. Of particular note is the recent work by Li and Ruckenstein [8], where adsorption isotherms are derived for mono- and bilayer adsorbed ionic surfactants on a charged surface, using molecular thermodynamic concepts similar to those employed in the present work. The other theoretical approach is based on self-consistent field models (see Koopal [11] for a review of this theory). These calculations were also limited to consideration of only lamellar structures. On the experimental side, adsorption isotherms have been measured for many different systems (see, for example, references [12–14]). The most important result is that the process of surface aggregation takes place at critical aggregate concentrations (CAC) much lower than the bulk-phase critical micelle concentration (CMC). This indicates that the aggregates are truly self-assembled on the surface, and they are not micelles formed in the bulk which get adsorbed on the surface.

Early studies were unable to explore the microstructure of surface aggregates. It was postulated that a continuous monolayer of surfactant forms on hydrophobic surfaces whereas a continuous bilayer forms on hydrophilic surfaces. In the past few years, investigators have begun to use high resolution scanning probe and atomic force microscopy (AFM) to directly visualize the structure of aggregates formed on a variety of surfaces, and under various solution conditions [15]. Many of these studies have focused on the surface aggregation of ionic surfactants on hydrophobic, atomically smooth graphite. The crystal lattice and the resulting anisotropy of its interactions with linear alkyl chains is postulated to be the defining feature that determines the morphology of aggregates on graphite surface [15]. Cationic alkyltrimethylammonium halide has been observed to form hemicylinders on graphite at surfactant concentrations on the order of the bulk-phase CMC [16–18]. For concentrations below 10% of the bulk CMC, AFM images are interpreted to be low surface density adsorbed monolayers with the surfactant molecules oriented such that only the tails are in contact with the surface [16]. Direct visualization of the surface aggregates of anionic sodium dodecyl sulfate (SDS) has also shown hemicylinders forming on graphite [19,20]. The addition of dodecanol co-surfactant to SDS solution causes a microstructural change from hemicylinders to a mixture of swollen hemicylinders and lamellae [20].

The microstructure of zwitterionic dodecyl dimethylammonio-propanesulfonate (DDAPS) aggregates on graphite was investigated by Ducker and Grant [21] via atomic force microscopy. They observed parallel stripes on the surface and interpreted them as being hemicylindrical aggregates. The microstructure of various nonionic surfactant aggregates have been observed via atomic force microscopy on the surfaces of both graphite and silica treated with diethyloctylchlorosilane (DEOS) to render it hydrophobic [22–24]. The latter surface differs from that of graphite because it is amorphous and isotropic in contrast to the anisotropy of the graphite surface. Patrick et al. [22] observed, for surfactants with polyethylene oxide head groups on graphite, a transition from lamellar to hemicylindrical structures as the ethylene oxide chain length is increased. Conversely, Grant et al. [24] observed for the same system a transition from continuous lamellae for short hydrocarbon tail lengths to hemicylinders at large tail lengths. Holland et al. [23] observed the formation of hemicylindrical aggregates of nonionic disaccharide surfactants on graphite. Some preliminary results for the adsorption of nonionic surfactants on the surface of DEOS treated silica indicate the formation of continuous monolayers [24].

The AFM studies mentioned above were all conducted at surfactant concentrations well above the bulk CMC. As mentioned before, the CAC for the formation of surface aggregates is typically much smaller than the bulk CMC. It is possible that the equilibrium aggregates which exist on the surface at concentrations near the CAC can have microstructures that deviate significantly from those seen via AFM at high surfactant concentrations. As yet, there has been no attempt to experimentally investigate the possibility of surface shape transitions as a function of surfactant concentration.

Shinto et. al. [25] have recently reported a molecular dynamics study of surfactant aggregation at a solid surface. They were able to qualitatively predict the formation of surface aggregates using a simplified model of surfactant molecules. To date, there has been no attempt to model the self-assembly behavior of surfactants on a hydrophobic surface, with a view to predict the microstructure of the surface aggregates. To address this need, we propose here a theoretical model based on molecular thermodynamics for the self-assembly of various surfactants at isotropic, hydrophobic solid surfaces. The approach is an extension of that proposed originally for self-assembly in bulk solution by Nagarajan and Ruckenstein [27]. Modifications have been incorporated to account for the interaction of the solvent and surfactant molecules with the hydrophobic surface. In the companion paper which follows, the formation of surface aggregates on hydrophilic surfaces is treated.

2. Thermodynamics of aggregation

The general principles of thermodynamics of aggregation are well established [26–29] and the relevant results are briefly mentioned below. The surfactant system can generate aggregates of various shapes (see Section 3) with all possible aggregation numbers. At equilibrium, the Gibbs free-energy of the system must be a minimum and this condition leads to the size distribution equation for aggregates of any shape:

$$X_g = X_1^g \exp\left(-\frac{g\Delta\mu_g^0}{kT}\right) \quad (1)$$

where X_g is the mole fraction of aggregates of size g, X_1 is the mole fraction of singly dispersed surfactant, and $\Delta\mu_g^0$ is the difference in standard chemical potentials between a surfactant molecule present in an aggregate of size g and a singly dispersed surfactant in solution.

For small values of g, the aggregates are spheres or globules (full in bulk solution or half on surfaces). As g increases, a transition from spherical or globular structures to (full or half) rodlike structures occurs. These large aggregates can be approximated as having a cylindrical middle with $(g-g_{cap})$ molecules and spherical endcaps with g_{cap} molecules. Under these conditions, Eq. (1) becomes

$$X_g = \left(\frac{1}{K}\right)Y^g, \quad Y = X_1 \exp\left(-\frac{\Delta\mu_{cyl}^0}{kT}\right),$$
$$K = \exp\left[g_{cap}\left(\frac{\Delta\mu_{cap}^0 - \Delta\mu_{cyl}^0}{kT}\right)\right] \quad (2)$$

where $\Delta\mu_{cap}^0$ and $\Delta\mu_{cyl}^0$ are analogs of $\Delta\mu_g^0$ and refer to the molecules in the spherical endcaps and cylindrical middle of the aggregate, respectively. The parameter K measures the free-energy advantage of molecules that are in the cylindrical section of the aggregate compared to those in the endcaps and Y measures the possibility of occurrence of rodlike aggregates at a given concentration X_1. Previous studies [27–29] have shown that K should be in the range of 10^8–10^{12} for polydispersed rodlike micelles to form at physically reasonable surfactant concentrations. Further, if rodlike micelles are formed, then Y should tend to unity.

The critical concentration corresponding to the formation of surface aggregates is referred to as the critical aggregate concentration (CAC) analogous to the CMC in bulk solutions. Although the CAC and various average aggregation numbers can be precisely estimated by calculating the concentrations of each aggregate using the formal size distribution equation, a more efficient and computationally simpler method is used here. If one assumes that the aggregate size distribution is narrow, then the distribution can be approximated by a single aggregate size that corresponds

to the maximum in the aggregate concentration. The average aggregation number is taken to be that value of the aggregation number g at which the aggregate concentration X_g is a maximum. The CAC is then estimated as $X_1 = gX_{g,\max} = X_{CAC}$.

This simplified approach is not appropriate, however, when cylindrical aggregates form since the size distribution will be quite broad. For this case, the standard chemical potential $\Delta\mu^0_{cyl}$ is calculated by its minimization with respect to the radius of the cylinder. $\Delta\mu^0_{cap}$ and g_{cap} corresponding to the endcaps are subsequently calculated by the minimization of $\Delta\mu^0_{cap}$ with respect to the radius of the endcap, which is generally allowed to differ from that of the cylindrical part. The sphere-to-rod transition parameter, K, is then calculated using Eq. (2) from which the weight and number average aggregation numbers can be estimated [28]. The CAC is taken equal to X_1 when $Y = 1$ in Eq. (2) yielding $X_1 = X_{CAC} = \exp(\Delta\mu^0_{cyl}/kT)$. The formation of planar aggregates is investigated by minimizing the free-energy difference $\Delta\mu^0_{lam}$ corresponding to an infinite lamella. The CAC corresponding to the formation of lamellar aggregates is calculated as $X_1 = X_{CAC} = \exp(\Delta\mu^0_{lam}/kT)$.

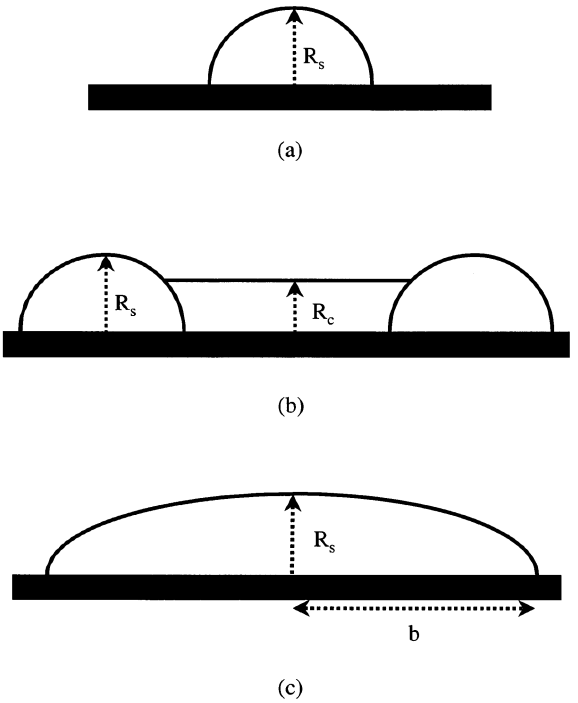

Fig. 1. Schematic representation of the structures of surfactant aggregates on a hydrophobic surface. The structures formed include hemispherical aggregates (a), hemicylindrical aggregates (b), and hemi-oblate ellipsoid aggregates (c). Continuous monolayers are not shown in this figure.

3. Geometrical properties of surface aggregates

To proceed with the calculation of the aggregation behavior of surfactants at a solid surface, models for the free-energy differences associated with aggregation are necessary. This requires specification of the shapes of the aggregates and their geometrical characteristics. For all shapes and sizes of aggregates, the hydrophobic cores are taken to be entirely composed of surfactant tails. The volume of the core is thus determined by the number of surfactant molecules g in the aggregate and the volume v_s of an individual surfactant tail. The aggregate shapes must conform to molecular packing constraints such that at least one dimension should be smaller than or at most equal to l_s, where l_s is the extended length of the surfactant tail. For hydrophobic surfaces, hemispherical, hemicylindrical, and monolayer disklike aggregates of both finite and infinite extent are considered (see Fig. 1). The geometrical relations for each kind of aggregate shape are given below. Two important area variables to note below are the aggregate core-water contact area per molecule (a_s) and the aggregate core-solid surface contact area per molecule (a_t).

3.1. Hemispherical aggregates

Small aggregates of aggregation number g are considered to be hemispherical (see Fig. 1(a)) with a hydrophobic core radius R_s, total volume V_g and surface area A_g.

$$V_g = gv_s = \frac{2\pi R_s^3}{3}, \quad A_g = ga_s = 2\pi R_s^2 \tag{3}$$

where a_s denotes the aggregate core-water contact area per molecule. A geometrical packing factor is defined as

$$P = \frac{V_g}{A_g R_s} = \frac{v_s}{a_s R_s} = \frac{1}{3} \quad (4)$$

which is invoked later for the estimation of chain packing free-energies. The area of the aggregate core that is in contact with the solid surface is πR_s^2. Therefore, the aggregate core-solid surface contact area per molecule, a_t, is

$$a_t = \frac{\pi R_s^2}{g} = \frac{3v_s}{2R_s} \quad (5)$$

This is required to determine the free-energy of interaction between the surface aggregate and the surface.

3.2. Hemicylindrical aggregates

3.2.1. Rodlike part

The cylindrical middle portion of a hemicylindrical aggregate is essentially half of an infinitely long cylindrical rod (see Fig. 1(b)), with a hydrophobic core radius R_c. The volume and total surface area per unit length of the cylinder are defined as

$$V_g = gv_s = \frac{\pi R_c^2}{2} \quad (6)$$

$$A_g = ga_s = \pi R_c \quad (7)$$

where g is the aggregation number per unit length of cylinder. The molecular packing factor is defined as before by

$$P = \frac{V_g}{A_g R_c} = \frac{v_s}{a_s R_c} = \frac{1}{2} \quad (8)$$

The aggregate core-solid surface contact area per molecule is then

$$a_t = \frac{2R_c}{g} = \frac{4v_s}{\pi R_c} \quad (9)$$

3.2.2. Endcaps

The two ends of the rodlike aggregate are considered to be parts of hemispheres (see Fig. 1(b)). The endcaps are allowed to have a radius R_s which is different from the radius R_c of the rodlike middle. The total volume V_g and the surface area A_g of the two endcaps together can be calculated from

$$V_g = gv_s = \frac{4\pi R_s^3}{3} - \frac{\pi H^2}{3}(3R_s - H) \quad (10)$$

$$A_g = ga_s = 4\pi R_s^2 - 2\pi R_s H \quad (11)$$

where

$$H = R_s - \sqrt{R_s^2 - R_c^2} \quad (12)$$

The molecular packing factor is defined as before, $P = V_g/A_g R_s$, and is always greater than 1/3. The aggregate core-solid surface contact area per molecule is

$$a_t = \frac{3v_s(2\pi - \theta + \sin\theta)}{\pi\left[4R_s - \frac{H^2}{R_s^2}(3R_s - H)\right]} \quad (13)$$

where θ denotes

$$\theta = 2\sin^{-1}\frac{R_c}{R_s} \quad (14)$$

3.3. Planar disklike aggregates

We consider aggregates having finite disklike structures and also continuous monolayers. Israelachvili et al. [29] have previously shown that in order for a disklike micelle to be finite, the central part of the disk must have some amount of curvature; a disklike structure with a planar center will always assume an infinite extent, based on free-energy considerations. Ellipses of revolution were suggested for these finite aggregate shapes. Here, the geometrical properties of such an aggregate shape are assumed equal, on the average, to those of an oblate ellipsoid (see Fig. 1(c)). Two geometrical variables are needed to define the oblate ellipsoids, namely the thickness of the monolayer, R_s, and the radial extent of the disk, b. It is clear that the average area per amphiphile of the aggregate will be different from the local areas per amphiphile in the circumferential edges and central parts of these aggregates.

3.3.1. Monolayer (infinite lamella)

The structure of a continuous monolayer is identical to that of an infinite lamella with thickness R_s The total volume and surface area of the aggregate per unit area of surface are calculated as

$$V_g = gv_s = R_s \tag{15}$$

$$A_g = ga_s = 1 \tag{16}$$

where g is the aggregation number per unit surface area. The molecular packing factor, $P = V_g/A_gR_s$, is equal to unity. The aggregate core-solid surface contact area per molecule is

$$a_t = \frac{1}{g} = \frac{v_s}{R_s} \tag{17}$$

3.3.2. Hemi-oblate ellipsoid (finite disk)

For hemi-oblate ellipsoids (see Fig. 1(c)), the semi-minor axis is determined by the extended length of the surfactant tails, i.e. $R_s = l_s$ while the semi-major axis is denoted by b. The total volume and surface area are calculated as

$$V_g = gv_s = \frac{2\pi R_s b^2}{3} \tag{18}$$

$$A_g = ga_s = \pi b^2\left[1 + \frac{1-E^2}{2E}\ln\left(\frac{1+E}{1-E}\right)\right] \tag{19}$$

where the eccentricity is defined as

$$E = \left[1 - \left(\frac{R_s}{b}\right)^2\right]^{1/2} \tag{20}$$

The molecular packing factor, $P = V_g/A_gR_s$, will always be greater than 1/3. The aggregate core-solid surface contact area per molecule is

$$a_t = \frac{\pi b^2}{g} = \frac{3v_s}{2R_s} \tag{21}$$

To facilitate later calculations of the ionic contribution to the overall free-energy of aggregation, an equivalent radius R_{eq} is defined as the radius of a hemisphere of equivalent volume,

$$R_{eq} = \left(\frac{3V_g}{2\pi}\right)^{1/3} \tag{22}$$

4. Free-energy of formation of surface aggregates

In order to calculate the equilibrium properties of the surface aggregates, a detailed representation of the standard free-energy difference $\Delta\mu_g^0$ between a surfactant molecule in an aggregate of size g and one in the singly dispersed state is desired. Following the approach of Tanford [26], this free-energy can be decomposed into a number of contributions on the basis of molecular considerations. Explicit equations for the various contributions have been developed in detail before [27] in the context of aggregation in solution and hence only the final expressions are given below, with appropriate modifications made for surface aggregates. One can refer to [27,28] for the detailed derivations of the free-energy expressions.

4.1. Transfer of the surfactant tail

The transfer free-energy of the surfactant tail as a function of temperature T (in K) is given [27,28] for CH_2 groups by

$$\frac{(\Delta\mu_g^0)_{tr}}{kT} = 5.85\ln T + \frac{896}{T} - 36.15 - 0.0056T \tag{23}$$

and for CH_3 groups by

$$\frac{(\Delta\mu_g^0)_{tr}}{kT} = 3.38\ln T + \frac{4064}{T} - 14.13 - 0.02595T \tag{24}$$

4.2. Deformation of the surfactant tail

For hemispherical aggregates, we can write [27,28]

$$\frac{(\Delta\mu_g^0)_{def}}{kT} = \frac{9P\pi^2}{80}\frac{R_s^2}{NL^2} \tag{25}$$

where N is the number of segments in the tail ($N = l_s/L$) and L is the characteristic segment length. The effective segment is taken to consist of 3.6 methylene units and the corresponding segment length is taken to be 0.46 nm consistent with the close packing of polymethylene chains in the liquid state. The above relation is used also for the endcaps of rodlike aggregates. For hemicylindrical rods, the coefficient 9 is replaced by 10, and the radius R_s is replaced by the cylinder radius, R_c The coefficient 10 is also used for infinite monolayer lamellar and finite monolayer disklike structures, with R_s being the layer thickness (see [27,28] for details).

4.3. Formation of aggregate core/water interface

This free-energy contribution is calculated [27,28] as the product of the aggregate core surface area in contact with water, and an effective interfacial tension, i.e.

$$\frac{(\Delta\mu_g^0)_{\text{int}}}{kT} = \frac{\gamma_{\text{agg}}}{kT}(a_s - a_0) \tag{26}$$

where a_s is the area per molecule of the hydrophobic core/water interface, and a_0 is the area that is shielded from contact with water by the polar head group. The aggregate core/water interfacial tension, γ_{agg} is taken to be the interfacial tension γ_{sw} between water and an aliphatic hydrocarbon with the same molecular weight as the surfactant tail. Details of estimating the molecular constants a_0 and γ_{sw} are given in [27,28].

4.4. Head group steric interactions

The steric repulsions among the head groups at the aggregate/water interface provide a free-energy contribution given by [27,28]

$$\frac{(\Delta\mu_g^0)_{\text{steric}}}{kT} = -\ln\left(1 - \frac{a_p}{a_s}\right) \tag{27}$$

where a_p is the cross-sectional area of the head group.

4.5. Head group dipole interactions

For zwitterionic surfactants, the dipole–dipole interactions between the head groups at the aggregate/water interface are calculated from [27,28]

$$\frac{(\Delta\mu_g^0)_{\text{dipole}}}{kT} = \frac{2\pi e^2 R_s}{\epsilon a_\delta kT}\frac{d}{R_s + \delta + d} \tag{28}$$

where e is the electronic charge, ϵ is the dielectric constant of the solvent (taken to be that of pure water), d is the dipole length, and δ is the distance from the core surface to the location of the dipole. The above equation is used for hemispheres, the endcaps of hemicylinders, and disklike aggregates (using R_{eq}) For infinite cylinders,

$$\frac{(\Delta\mu_g^0)_{\text{dipole}}}{kT} = \frac{2\pi e^2 R_c}{\epsilon a_\delta kT}\ln\left(1 + \frac{d}{R_c + \delta}\right) \tag{29}$$

and for infinite lamella,

$$\frac{(\Delta\mu_g^0)_{\text{dipole}}}{kT} = \frac{2\pi e^2 d}{\epsilon a_\delta kT} \tag{30}$$

4.6. Head group ionic interactions

For ionic surfactants, the electrostatic free-energy of head group interactions at aggregate/water interface is given by [27,28]

$$\begin{aligned}\frac{(\Delta\mu_g^0)_{\text{ionic}}}{kT} = 2\Bigg\{&\ln\left[\frac{S}{2} + \left(1 + \left(\frac{S}{2}\right)^2\right)^{1/2}\right] \\ &- \frac{2}{S}\left[\left(1 + \left(\frac{S}{2}\right)^2\right)^{1/2} - 1\right] \\ &- \frac{2C}{\kappa S}\ln\left[\frac{1}{2} + \frac{1}{2}\left(1 + \left(\frac{S}{2}\right)^2\right)^{1/2}\right]\Bigg\}\end{aligned} \tag{31}$$

where

$$S = \frac{4\pi e^2}{\epsilon\kappa a_\delta kT} \tag{32}$$

and κ is the reciprocal Debye length. The last term in Eq. (31) represents a correction for the curvature of the interface, with C, given by

$$C = \frac{2}{R_s + \delta}, \frac{2}{R_{\text{eq}} + \delta}, \frac{1}{R_c + \delta} \tag{33}$$

for hemispheres/hemispherical endcaps, disklike aggregates with an equivalent radius, R_{eq} defined before, and infinite rodlike aggregates, respectively. Note that for the planar portion of the disklike aggregates, and for infinite lamella C will be 0.

4.7. Solid surface/aggregate core interactions

This is the only additional contribution for surface aggregates on hydrophobic surfaces since all other free-energy contributions are relevent also for aggregates in solution. This attractive contribution arises due to the displacement of water by the hydrophobic core of the aggregate on the solid surface. This interaction free-energy is taken to be the product of the aggregate core-solid surface contact area per molecule, a_t, and the difference in the interfacial tension, $\gamma \simeq \gamma_{\text{sur}-\text{w}} - \gamma_{\text{sur}-\text{agg}}$

$$\frac{(\Delta\mu_g^0)_{\text{surface}}}{kT} = -\frac{\gamma}{kT}a_t \tag{34}$$

where γ is referred to later as the displacement tension accounting for the replacement of solid surface-water contact ($\gamma_{\text{sur}-\text{w}}$) by the solid surface/aggregate core contact ($\gamma_{\text{sur}-\text{agg}}$) For a surface that is entirely hydrocarbon in nature, $\gamma_{\text{sur}-\text{w}} \simeq 50$ dynes cm^{-1} and $\gamma_{\text{sur}-\text{agg}} \simeq 0$ dynes cm^{-1} and hence a limiting value of $\gamma \simeq 50$ dynes cm^{-1} can be realized. For all positive values of γ, $(\Delta\mu_g^0)_{\text{surf}}$ will contribute favorably to the formation of surface aggregates. Furthermore, the higher the displacement tension, γ, the more favorable the formation of surface aggregates.

5. Prediction of aggregation behavior

5.1. Computational technique

The size distribution equation, in conjunction with the contributions to the free-energy of micellization and the geometrical properties of the aggregates allows one to calculate various properties of the system. In the aggregate size distribution, $\Delta\mu_g^0$ is the sum of a number of contributions

$$\Delta\mu_g^0 = (\Delta\mu_g^0)_{\text{trans}} + (\Delta\mu_g^0)_{\text{def}} + (\Delta\mu_g^0)_{\text{inter}} + (\Delta\mu_g^0)_{\text{steric}} + (\Delta\mu_g^0)_{\text{dipole}} + (\Delta\mu_g^0)_{\text{ionic}} + (\Delta\mu_g^0)_{\text{surf}} \tag{35}$$

where $(\Delta\mu_g^0)_{\text{dipole}}$ is included if the surfactant is zwitterionic, $(\Delta\mu_g^0)_{\text{ionic}}$ if the surfactant is ionic, and neither if the surfactant is nonionic. All contributions other than $(\Delta\mu_g^0)_{\text{surf}}$ are present in the case of bulk aggregates and the expressions for bulk aggregates and their geometrical properties are described in detail in [27,28]. These are employed for investigation of bulk aggregation properties.

The computational procedure is the same for both bulk aggregates and surface aggregates. For hemispheres and finite disklike aggregates, an initial guess for X_1 is assumed (typically $X_1 = 0.002$). The minimum of $\Delta\mu_g^0$ with respect to the independent geometrical variable (typically R_s) is found using a golden section search in one dimension. The surfactant concentration X_1 is then updated by noting that $X_1 = gX_g$ at the CAC. The aggregate size distribution Eq. (1) can then be rearranged to give

$$X_1 = \exp\left(\frac{\ln g - \frac{g\Delta\mu_g^0}{kT}}{1-g}\right) \tag{36}$$

The minimum of $\Delta\mu_g^0$ is then found at the new value of X_1 and the process is repeated until X_1 has converged to within a tolerance of 10^{-6} (i.e. the difference between two successive iterated values of X_1 is less than $10^{-6}X_1$).

For rodlike aggregates at a given X_1, both $(\Delta\mu^0)_{\text{cap}}$ and $(\Delta\mu^0)_{\text{cyl}}$ must be minimized. The value of X_1 is then updated by noting that at the CAC

$$X_1 = \exp\left(\frac{\Delta\mu_{\text{cyl}}^0}{kT}\right) \tag{37}$$

Similarly for infinite lamellar aggregates, $(\Delta\mu^0)_{\text{lam}}$ must be minimized at a given X_1. The value of X_1 is then updated in a manner similar to that for rodlike aggregates.

Due to the fixed point nature of this procedure, the convergence rate will never be better than quadratic, but nevertheless the CAC was found to rapidly converge in no more than 40 iterations, regardless of the initial conditions, requiring at most a few seconds of CPU time on an IBM RS/6000 workstation.

5.2. Estimation of molecular constants

Predictive calculations have been carried out for ionic, zwitterionic, and nonionic surfactants. All of the surfactant tails considered here are composed of aliphatic hydrocarbons. The associated molecular constants are the volume, v_s, and the extended length, l_s, of the tail. As for the head group, the molecular constants that are required are the cross-sectional area, a_p, for all types, the distance, δ, from the core surface to where the counterion is located for ionic types, and the dipole length, d, and the distance, δ, from the core surface to where the dipole is located for zwitterionic types. It should be emphasized that all molecular parameters are simply functions of the molecular structure of the surfactant in question, and are not adjustable parameters. The molecular

Table 1
Molecular constants for surfactant head groups.

Surfactant head group	a_p (nm^2)	a_0 (nm^2)	δ (nm)	d (nm)
Sodium alkyl sulfate	0.17	0.17	0.545	–
N-Alkylbetaine	0.30	0.21	0.07	0.5
Nonionic	0.45	0.21	–	–

constants used here (Table 1) are the same as those employed in [27,28] for predicting bulk aggregation behavior. The constant for the nonionic surfactant is selected only for simulation purposes.

5.3. Model predictions

5.3.1. General aggregation behavior

The predicted and experimentally observed aggregation behavior of the three types of surfactants under consideration is summarized in Table 2 based on calculations performed taking the displacement tension to be $\gamma = 50$ and 10 dynes cm^{-1}. The experimental observations are those made via AFM at surfactant concentrations on the order of the bulk CMC, whereas the model predictions correspond to surfactant concentrations at the CAC. In general, experiments show that continuous lamellae and hemicylinders form

Table 2
Surface aggregation behavior on hydrophobic surfaces

Surfactant/surface	System conditions	Surface microstructure	Reference
(A) Experimental results			
CTAB/graphite	Low concentration	Monolayers	[16]
	High concentration	Hemicylinders	[16,18]
SDS/graphite		Hemicylinders	[20]
	Dodecanol	Swollen hemicylinders/lamellae	[20]
	NaCl	Hemicylinders	[19]
DDAPS/graphite		Hemicylinders	[19]
C_nE_x/graphite	Large EO	Lamellae	[22]
	Small EO	Hemicylinders	[22]
Dissacharide/graphite		Hemicylinders	[23]

Surfactant	System conditions	Bulk microstructure	Surface microstructure
(B) Model predictions at CAC: $\gamma = 50$ dynes cm^{-1}			
Ionic	Small n_c	Spheres	Hemispheres
	Large n_c	Globules/small rods	Small hemicylinders
Nonionic	Small n_c	Globules	Small hemicylinders
	Large n_c	Small rods	Large hemicylinders
Zwitterionic	Small n_c	Globules	Small hemicylinders
	Large n_c	Small rods	Large hemicylinders
(C) Model predictions at CAC: $\gamma = 10$ dynes cm^{-1}			
Ionic	Small n_c	Spheres	Hemispheres
	Large n_c	Globules/small rods	Hemispheres
Nonionic	Small n_c	Globules	Finite disks
	Large n_c	Small rods	Small hemicylinders
Zwitterionic	Small n_c	Globules	Small hemicylinders
	Large n_c	Small rods	Monolayers

on hydrophobic surfaces. The formation of hemicylinders on the surface of graphite has been attributed to the anisotropy of the surface morphology implying that on isotropic surfaces hemicylinders may not form and only monolayers may be possible. In our model, only isotropic surfaces are considered and all surface effects are contained within the single parameter, displacement tension γ. The model predictions show two opposing trends for different values of γ. For $\gamma = 50$ dynes cm^{-1}, the surface aggregates are smaller than the bulk aggregates for ionic surfactants whereas the surface aggregates are larger than the bulk aggregates for nonionic and zwitterionic surfactants. In contrast, for $\gamma = 10$ dynes cm^{-1}, the surface aggregates are smaller than the bulk aggregates for all types of surfactants. Also, interestingly, the model predicts the formation of continuous monolayers only for zwitterionic surfactant on isotropic hydrophobic surfaces when the surfactant concentration is at the CAC. The contrasting surface aggregation behavior for the two values of γ and the important influence of the surfactant concentration on surface aggregate morphologies will be elaborated below.

The predicted surface aggregation behavior is most easily interpreted by considering the following simplified representation for the free-energy of aggregation

$$\Delta\mu_g^0 = \text{const} + a_s\left(\gamma_{HC-W} - \gamma\frac{a_t}{a_s}\right) + \frac{\alpha}{a_s} \tag{38}$$

where the first term represents the transfer free-energy, the second term is the free-energy change associated with the formation of the aggregate core/water interface and the aggregate core/solid surface interface, and the final term represents the free-energy change due to head group repulsion. All the variables have been defined before, but for α, which is a constant, representing the various types of head group repulsion. Note that this is essentially Tanford's original equation [26], with a slight modification for the formation of the aggregate core/solid surface interface. The ratio a_t/a_s is simply a constant, and the geometrical relations in Section 3 show that $1/2 \le a_t/a_s \le 2/\pi$ for all surface aggregates of finite size. When Eq. (38) is minimized with respect to a_s, the equilibrium area a_s is obtained:

$$a_s = \left(\frac{\alpha}{\gamma_{HC-W} - \gamma\frac{a_t}{a_s}}\right)^{1/2} \tag{39}$$

This equation shows that since γ is always positive and can be of the order of γ_{HC-W}, surface aggregates will always have a larger area per molecule, a_s, than their bulk-phase counterparts. In light of the geometrical relations for spherical and globular micelles described earlier, this implies that the aggregation number, g, must decrease for any surface aggregate, relative to bulk-phase micelles. Note that this equation applies also to bulk aggregates but with $a_t/a_s = o$.

This analysis explains well the results for ionic surfactants with small n_c, when only spherical or finite disklike surface aggregates are formed. However, as indicated in Table 2, the other systems under consideration (nonionic and zwitterionic surfactants) can form larger, hemicylindrical aggregates at the solid surface. The behavior of nonionic and zwitterionic surfactants can also be interpreted using the same free-energy Eq. (38). The sphere-to-rod transition parameter, K, is governed by the free-energy difference $(\Delta\mu_g^0)_{cap} - (\Delta\mu_g^0)_{cyl}$. This free-energy difference can be rewritten (based on Eq. 38) as

$$(\Delta\mu_g^0)_{cap} - (\Delta\mu_g^0)_{cyl} = \gamma_{HC-W}(a_{cap} - a_{cyl}) + \alpha\left(\frac{1}{a_{cap}} - \frac{1}{a_{cyl}}\right) - \gamma\left(\frac{1}{2}a_{cap} - \frac{2}{\pi}a_{cyl}\right) \tag{40}$$

where the first term is due to aggregate core/solvent interface formation, the second term is due to head group repulsion, and the last term accounts for the displacement of water by the aggregate core at the solid surface. In order for K to be sufficiently large, which is a necessary condition for the formation of hemicylindrical structures, the free-energy difference $[(\Delta\mu_g^0)_{cap} - (\Delta\mu_g^0)_{cyl}]/kT$ must be positive, but need not be large. Indeed, for a typical value of $g_{cap} = 40$, the free-energy difference need only be $\simeq 0.5$ kT in order for K to be large enough ($\ln K \sim 20$ in this case) for rods to form.

Although one must be careful when making quantitative predictions with this simplified approach (Eqs. 38 or 40), some generalizations can be made in light of the model predictions mentioned in Table 2. The areas a_{cap} and a_{cyl} of hemicylindrical aggregates are determined by α, γ, and γ_{HC-W}. Given the geometry of rodlike aggregates a_{cap} will always be greater than a_{cyl}. This guarantees that, in Eq. (40), the first term is positive and the second term is negative. However, the last term in Eq. (40) is the factor that determines the size of the hemicylindrical surface aggregates compared to the bulk, since this term is the only addition when surface aggregation takes place. The first term in Eq. (40) contributes to an increase in K whereas the second term contributes to a decrease in K. The third term can lead to an increase or a decrease in K. Specifically, since γ is always positive, if $a_{cap} > 1.27a_{cyl}$, then K will be smaller for surface aggregates compared to bulk, the *decrease* in K being larger for large values of γ. Conversely, if $a_{cap} < 1.27a_{cyl}$, then K will be larger for surface aggregates compared to bulk, the *increase* in K being larger for large values of γ.

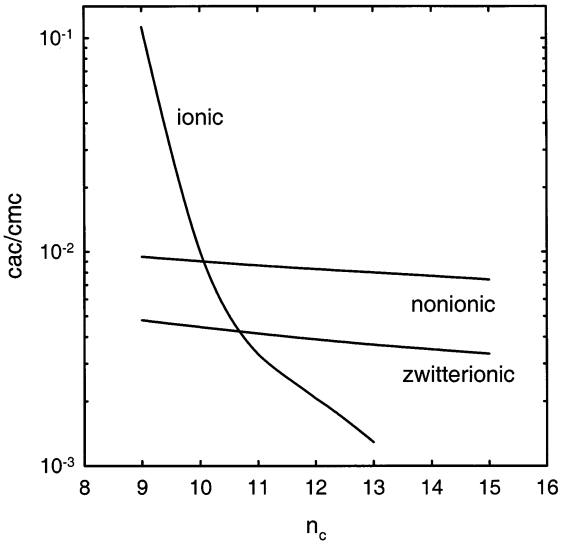

Fig. 2. Dependence of the critical aggregate concentration (normalized by the bulk phase critical micelle concentration) on the surfactant tail length for ionic sodium alkyl sulfates, zwitterionic *N*-alkylbetaines, and a nonionic surfactant (with $a_p = 0.45$ nm^2) for displacement tension $\gamma = 50$ dynes cm^{-1}.

One may note that α is smaller for nonionic and zwitterionic surfactants compared to that for ionic surfactants. Therefore, for ionic surfactants, the head group repulsion term in Eq. (40) will provide a large negative contribution, thus lowering the value of K. This can explain why hemicylindrical surface aggregates of ionic surfactants are generally predicted to be smaller than the corresponding bulk structures, while hemicylindrical surface aggregates of zwitterionic and nonionic surfactants are generally predicted to be larger. However, as described earlier, this behavior is highly dependent on the value of γ. The value of K can be decreased by either decreasing the value of γ, or increasing the value of α. Conversely, the value of K can be increased by either increasing γ or decreasing α. Thus, the interplay between the head group repulsion term and the aggregate core/solid surface interface formation term determines whether the behavior shown by ionic surfactants or that shown by nonionic or zwitterionic surfactants at the two values of γ will occur. In general, we note that various aggregate shapes are predicted which do not depend on any special feature, such as anisotropy, of the surface.

5.3.2. Influence of surfactant tail length

In this section, we report some specific results for illustrative surfactant and solution conditions. The CAC values predicted at 25°C for anionic sodium alkyl sulfates, zwitterionic *N*-alkylbetaines, and a nonionic surfactant with $a_p = 0.45$ nm^2 are presented in Fig. 2 where the CAC values have been normalized by the corresponding bulk-phase CMC. All the calculated results discussed in this section have been obtained corresponding to a displacement tension γ of 50 dynes cm^{-1}. For all tail lengths and head groups, the CAC is predicted to be at least one order of magnitude lower than the bulk phase CMC, and is over two orders of magnitude lower for high n_c. Thus, surface aggregates are predicted to always form before their bulk-phase analogs. As a result of the increasing magnitude of the transfer free-energy with increasing n_c, the CAC decreases with increasing surfactant tail length, analogous to that for bulk-phase micellization. However, the CAC for ionic surfactants decreases at a faster rate as n_c

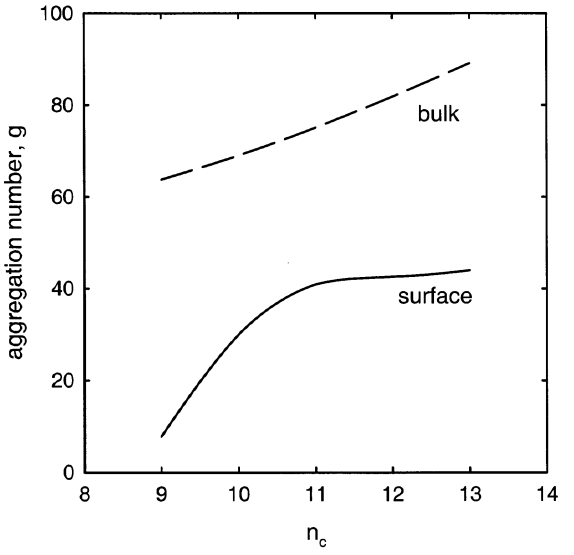

Fig. 3. Dependence of the aggregation number of the surface aggregates at the CAC, and bulk aggregates at the CMC on the surfactant tail length, n_c, for ionic sodium alkyl surfates for $\gamma = 50$ dynes cm^{-1}.

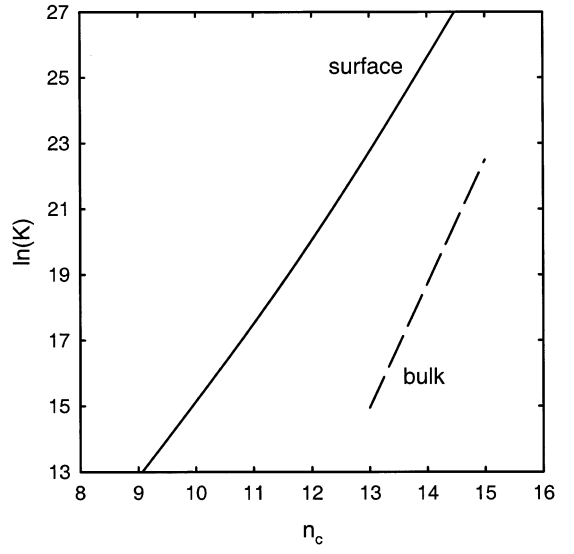

Fig. 4. Dependence of the sphere-to-rod transition parameter, K, for the surface aggregates at the CAC, and bulk aggregates at the CMC on the surfactant tail length, n_c, for zwitterionic N-alkylbetaines for $\gamma = 50$ dynes cm^{-1}.

is increased than for the other two types of surfactants.

The predicted average aggregation numbers at the CAC and CMC are plotted as functions of surfactant tail length for anionic sodium alkyl sulfates in Fig. 3. For all values of n_c, the surface structures are hemispherical, while the bulk micelles are globular. It is clear that the surface aggregates are smaller than their bulk-phase counterparts. The dependence of the sphere-to-rod transition parameter, K, on the surfactant tail length is shown in Fig. 4 for the zwitterionic N-alkylbetaine head group. In the bulk-phase, rodlike micelles are formed only above $n_c = 13$; below $n_c = 13$ globules are formed. In contrast to the trend observed with ionic surfactants, the surface aggregates of the zwitterionic surfactant are larger than the corresponding bulk phase micelles, as reflected by the larger value of K at any given value of n_c. Fig. 5 shows the dependence of K on n_c for a nonionic surfactant head group with $a_p = 0.45$ nm^2. In the bulk, rods form only above $n_c = 11$, whereas large hemicylinders form at the solid surface for all $n_c \geq 9$. As for zwitterionic surfactants, the surface aggregates have larger K values than that for the corresponding bulk-phase micelles. However, the difference in the magnitude of K between surface and bulk-phase aggregates is

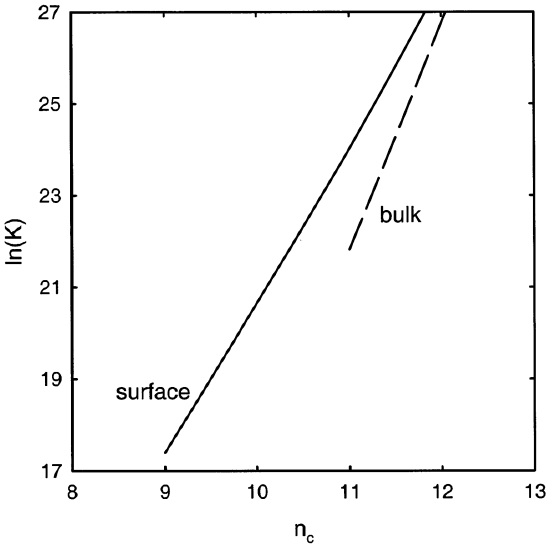

Fig. 5. Dependence of the sphere-to-rod transition parameter, K, for the surface aggregates at the CAC, and bulk aggregates at the CMC on the surfactant tail length, n_c, for a nonionic surfactant with $a_p = 0.45$ nm^2.

Table 3
(A) Minimum free-energy values for various surface microstructures of each type of surfactant with $n_c = 12$[a]

Surfactant	Microstructure	$\Delta\mu_g^0$ (kT)
Ionic	Hemisphere	−15.2
	Hemicylinder (cap)	−12.5
	Hemicylindrical (middle)	−11.0
	Finite monolayer	−10.2
	Infinite monolayer	−9.20
Zwitterionic	Hemicylinder (cap)	−13.9
	Hemicylindrical (middle)	−14.9
	Hemisphere	−13.5
	Finite monolayer	−13.4
	Infinite monolayer	−11.8
Nonionic	Hemicylinder (cap)	−15.5
	Hemicylindrical (middle)	−16.3
	Finite monolayer	−15.3
	Hemisphere	−15.1
	Infinite monolayer	−13.3

(B) Proposed concentration-dependent change based on the above free-energy estimates (valid for $n_c = 12$ and $\gamma = 40$ dynes cm^{-1})

Ionic	Zwitterionic	Nonionic
Hemisphere ($X_1 = $ CAC)	Hemicylinder ($X_1 = $ CAC)	Hemicylinder ($X_1 = $ CAC)
Hemicylinder ($X_1 \sim 67$ CAC)	Hemisphere ($X_1 \sim 4$ CAC)	Finite Disk ($X_1 \sim 2.7$ CAC)
Finite Disk ($X_1 \sim 148$ CAC)	Finite Disk ($X_1 \sim 4.5$ CAC)	Hemisphere ($X_1 \sim 3.3$ CAC)
Lamella ($X_1 \sim$ 403 CAC)	Lamella ($X_1 \sim 22$ CAC)	Lamella ($X_1 \sim 20$ CAC)

[a] Calculated results are for displacement tension $\gamma = 40$ dynes cm^{-1}.

appreciably smaller for the nonionic head group than for the zwitterionic surfactant of the same tail length.

5.3.3. Effect of surfactant concentration

Studies conducted with the goal of determining adsorption isotherms typically employ a large surface area of solids. Under these conditions, beyond the CAC, any increase in total surfactant concentration results in an increase in the concentration of surface aggregates, keeping the monomer concentration, X_1, nearly constant. In contrast, the total amount of surfactant necessary to saturate the solid surface in an AFM experiment is negligible because of its small surface area. This implies that an increase in the total concentration of surfactant in the system will cause a corresponding increase in the monomer concentration, X_1, because very little of the surfactant is incorporated into surface aggregates. A change in X_1 implies changing the chemical potential of the surfactant. Therefore, in interpreting and comparing the AFM results (obtained at total surfactant concentrations that are 10–1000 times the CAC) to the model predictions at the CAC, the effect of surfactant concentration must be considered.

Recall that Eq. (1) predicts the concentration of aggregates, X_g, to depend on the product of the concentration of singly dispersed surfactant, X_1, and the exponential of the standard state free-energy of aggregation. This immediately suggests that a free-energy penalty for forming a certain type of aggregate can be overcome by an increase in X_1. For instance, a single order of magnitude change in X_1 can overcome a free-energy difference of roughly 2.3 kT. The progression of free energies of aggregation of several types of surfactant with $n_c = 12$ are shown in Table 3A, where the illustrative calculations have been performed for a displacement tension $\gamma = 40$ dynes cm^{-1}. The progression of shapes of surface aggregates with increasing surfactant concentration is summarized in Table 3B corresponding to the aggregate free-energies listed in Table 3A. The most negative value of the free-energy implies the most favorable aggregate. One can envision a progression of microstructures as the surfactant concentration is increased, as depicted in Fig. 6 for an ionic surfactant in the absence of added salt. As the surfactant concentration is increased above the CAC, less energetically favorable structures may form at the interface. Focusing on the ionic sodium alkyl sulfate with $n_c = 12$ (Table 3A), it is clear that hemispheres are the most favorable microstructure, and the one that will initially form at a low concentration (i.e. at the CAC). However, ~ 4.2 kT separates the energies corresponding to hemispheres and hemicylinders in the

progression. According to Eq. (1), this corresponds to roughly a 67-fold increase of X_1 to achieve a surface shape transition. As indicated in Fig. 6, when X_1 is increased above the CAC, but below the concentration required to induce a shape transformation, the surface becomes saturated with aggregates of the original microstructure (i.e. X_g increases). When the concentration is further increased to 67 times the CAC, calculations indicate that it is possible to overcome the free-energy barrier for the formation of hemicylinders on the surface. Finally at highly elevated surfactant concentrations (403 times the CAC), it is possible for the hemicylindrical surface structures to transform into a monolayer uniformly covering the surface.

For the same surfactant, the CAC is predicted to be about three orders of magnitude smaller than the bulk CMC (CAC/CMC = 0.003). Wanless, Davey, and Ducker [20] reported that sodium dodecyl sulfate ($n_c = 12$) forms hemicylinders on graphite over a concentration range from about 1/3 to at least 10 times the bulk CMC. Although the model predicts the formation of hemispheres at the CAC, the experimental observations are consistent with the model predictions due to the effects of elevated surfactant concentration.

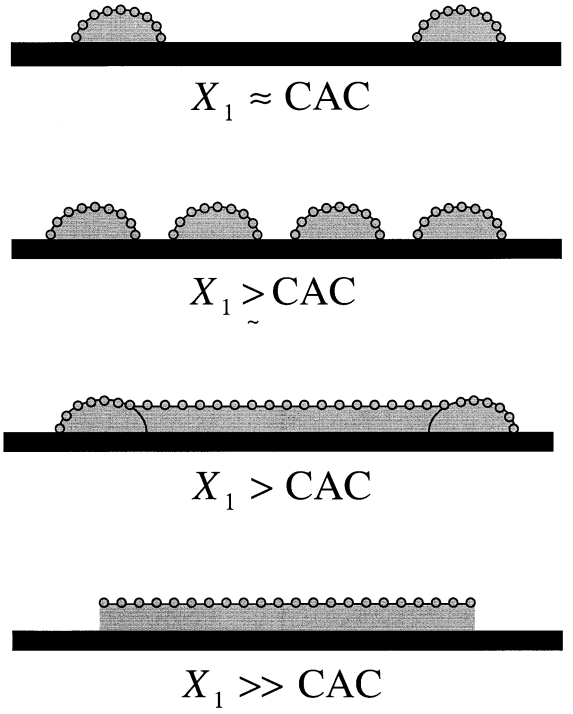

Fig. 6. Progression of aggregate microstructures as the concentration of singly dispersed ionic surfactant, X_1, is increased beyond the CAC for $n_c = 12$ and $\gamma = 40$ dynes cm^{-1}.

Although the above discussion has focused only on ionic surfactants, the concepts also apply to the other systems under consideration. The progression of free energies of aggregation for zwitterionic and nonionic surfactants are also shown in Table 3. In contrast to the case of ionic surfactants, the microstructure with the lowest free-energy of aggregation, and the one that will be present at the CAC is hemicylindrical for both of these surfactants. Thus, the progression of surface microstructures is somewhat different than that for ionic surfactants (Table 3B). At low surfactant concentrations (i.e. below the bulk CMC), widely separated hemicylinders will be present on the surface. As the surfactant concentration is increased, the hemicylinders will become more densely packed on the surface. Finally, as with ionic surfactants, at larger surfactant concentrations, uniform lamellar structures form. For intermediate concentrations, hemispherical and finite disklike structures are predicted. Table 3B is valid for the illustrative case with $n_c = 12$ and the displacement tension $\gamma = 40$ dynes cm^{-1}. It shows the variety of aggregate shapes that are possible as functions of surfactant concentration in a typical AFM study.

6. Conclusions

A theory of surfactant self-assembly at the interface between an isotropic hydrophobic solid surface and the solvent is developed. The model calculations require only the molecular properties of the surfactant, solvent, and the surface. The theory is based on the well established treatment of surfactant self-assembly in solution, with a new contribution added to the free-energy of surface aggregation to account for the interaction of the hydrophobic aggregate core with the solid surface. A single new parameter, displacement tension γ, that has units of dynes cm^{-1}, is introduced to

account for the replacement of solid surface-water contact by solid surface/aggregate core contact.

Model predictions are made for anionic sodium alkyl sulfates, zwitterionic *N*-alkylbetaines, and nonionic surfactants with head group cross-sectional area $a_p = 0.45$ nm^2. Due to the favorable energetics of the surface contribution to the free-energy of aggregation, the critical condition for self-assembly at the surface (the CAC) is always lower than the bulk CMC, and is typically more than an order of magnitude lower. At the CAC, surface aggregates of ionic surfactants are predicted to be smaller than their bulk-phase counterparts. On the other hand, surface aggregates of zwitterionic and nonionic surfactants can either be larger or smaller than their bulk-phase analogs, depending on the value of γ. The interplay between head group repulsion and aggregate core/solid surface interface formation determines whether the surface aggregates are smaller or larger than bulk aggregates.

Experimental observations of surface microstructures based on the AFM technique have been typically made at surfactant concentrations that are much larger than the CAC. Since the surface area of the solid in an AFM experiment is small, the total surfactant concentration is nearly identical to the monomer concentration, X_1. By increasing the chemical potential of the surfactant (by increasing the total surfactant concentration) it is possible to overcome the free-energy penalty in forming energetically unfavorable microstructures. This allows the possibility of energetically unfavorable microstructures existing at surfactant concentrations in excess of the CAC, such as those observed in AFM experiments. The model predicts various types of aggregate structures such as hemispheres, hemicylinders, finite disks, and infinite lamella to be possible depending upon the surfactant, solid surface, and surfactant concentration. The predictions are made for isotropic solid surfaces and suggest that the anisotropy of the graphite surface is not essential for the formation of such a rich variety of aggregate shapes. Future experiments on well defined isotropic surfaces and at various surfactant concentrations can aid in a quantitative test of the present theory.

Acknowledgements

We acknowledge the interesting AFM studies of Professors Ducker and Manne which stimulated this theoretical study. Conversations with Professor Ducker in the context of model development are gratefully acknowledged.

References

[1] B.M. Moudgil, H. Soto, P. Somasundaran, in: P. Somasundaran, B.M. Moudgil III (Eds.), Reagents in Mineral Processing, Marcel Dekker, New York, 1988, pp. 79–104.
[2] A.M. Gaudin, D.W. Fuerstenau, Trans. Am. Inst. Metall. Pet. Eng. 202 (1955) 958–962.
[3] J.H. O'Haver, L.L. Lobban, J.H. Harwell, E.A. O'Rear III, in: S.D. Christian, J.F. Scamehorn (Eds.), Solubilization in Surfactant Aggregates, Marcel Dekker, New York, 1995, pp. 227–295.
[4] J.H. Harwell, J.C. Hoskins, R.S. Schechter, W.H. Wade, Langmuir 1 (1985) 251–262.
[5] M.A. Yeskie, J.H. Harwell, J. Phys. Chem. 92 (1988) 2346–2352.
[6] P. Levitz, Langmuir 7 (1991) 1595–1608.
[7] H.P. Huinink, A. de Keizer, F.A.M. Leermakers, J. Lyklema, Langmuir 14 (1998) 2693–2701.
[8] B. Li, E. Ruckenstein, Langmuir 12 (1996) 5052–5063.
[9] J. Narkiewicz-Michalek, Ber. Bunsenges. Phys. Chem. 1 (1991) 85–95.
[10] B.-Y. Zhu, T. Gu, Adv. Colloid Interface Sci. 37 (1991) 1–32.
[11] L. Koopal, in: K. Esumi, M. Ueno (Eds.), Structure-Performance Relationships in Surfactants, Marcel Dekker, New York, 1997, pp. 395–469.
[12] F.J. Trogus, R.S. Schechter, W.H. Wade, J. Colloid Interface Sci. 70 (1978) 293–305.
[13] P.D. Bisio, J.G. Cartledge, W.H. Keesom, C.J. Radke, J. Colloid Interface Sci. 78 (1980) 225–234.
[14] J.F Scamehorn, R.S. Schechter, W.H. Wade, J. Colloid Interface Sci. 85 (1982) 463–478.
[15] S. Manne, G.G. Warr, In: S. Manne, G.G. Warr (Eds.), Supramolecular Structure in Confined Geometries, ACS Symposium Series No. 736, 1999; pp. 2–23.
[16] S. Manne, J.P. Cleveland, H.E. Gaub, G.D. Stucky, P.K. Hansma, Langmuir 10 (1994) 4409–4413.
[17] S. Manne, H.E. Gaub, Science 270 (1995) 1480–1482.
[18] S. Manne, Progr. Colloid Polym. Sci. 103 (1997) 226–233.
[19] E.J. Wanless, W.A. Ducker, J. Phys. Chem. 100 (1996) 3207–3214.
[20] E.J. Wanless, T.W. Davey, W.A. Ducker, Langmuir 13 (1997) 4223–4228.
[21] W.A. Ducker, L.M. Grant, J. Phys. Chem. 100 (1996) 11507–11511.

[22] H.N. Partick, G.G. Warr, S. Manne, I.A. Aksay, Langmuir 13 (1997) 4349–4356.
[23] N.B. Holland, M. Ruegsegger, R.E. Marchant, Langmuir 14 (1998) 2790–2795.
[24] L.M. Grant, F. Tiberg, W.A. Ducker, J. Phys. Chem. B 102 (1998) 4288–4294.
[25] H. Shinto, S. Tsuji, M. Miyahara, K. Higashitani, Langmuir 15 (1999) 578–586.
[26] C Tanford, The Hydrophobic Effect, second edition, Wiley-Interscience, New York, 1980.
[27] R. Nagarajan, E. Ruckenstein, Langmuir 7 (1991) 2934–2969.
[28] R. Nagarajan, in: K. Esumi, M. Ueno (Eds.), Structure-Performance Relationships in Surfactants, Marcel Dekker, New York, 1997, pp. 1–81.
[29] J.N. Israelachvili, J.D. Mitchell, B.W. Ninham, J. Chem. Soc. Faraday Trans. II 72 (1976) 1525.